THE JOURNAL OF PHYSICAL CHEMISTRY C

Article

pubs.acs.org/JPCC

Using ATTO Dyes To Probe the Photocatalytic Activity of Au–CdS Nanoparticles

Published as part of The Journal of Physical Chemistry virtual special issue "Mark S. Gordon Festschrift".

Ujjal Bhattacharjee,[†,‡] Long Men,[†,‡] Bryan A. Rosales,[†,‡] Samuel R. Alvarado,[†,§] Javier Vela,[†,‡] and Jacob W. Petrich*[,†,‡]

[†]Department of Chemistry and [‡]U.S. Department of Energy Ames Laboratory, Iowa State University, Ames, Iowa 50010, United States

Supporting Information

ABSTRACT: Metal–semiconductor nanohybrids (or heterostructures), such as Au–CdS, have become an important class of materials because of their role in photochemical hydrogen production and in other catalytic reactions. Here we report the results of photophysical studies of the interactions of these particles with ATTO dyes (ATTO 590 and 655), which are used as fluorescent probes in a wide range of spectroscopic techniques, most notably super-resolution microscopies. The most important feature of the Au–CdS particles is that they provide the possibility of selective excitation at either their CdS or their Au domains, which absorb preferentially at wavelengths shorter or longer than 500 nm, respectively, thus making possible an excited-state charge transfer reaction from ATTO. Fluorescence quenching of ATTO is dominated by charge transfer to either the CdS domain (λ_{ex} = 400 nm) or the Au domain (λ_{ex} = 570 nm). This quenching is quantified by steady-state and time-resolved absorption and fluorescence measurements, and its assignment is confirmed by electrochemical measurements. The results indicate that the ATTO dyes are sensitive and useful probes for measuring the photocatalytic activity of nanoparticles. Characterizing the nonradiative processes of the ATTO dyes in the presence of these catalytically active particles provides a means of gauging their utility in the wide range of spectroscopies in which they are employed.

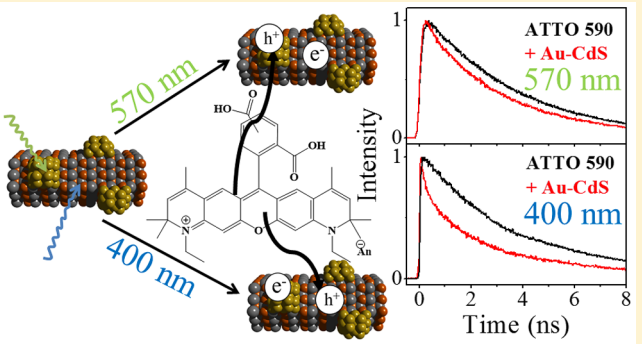

INTRODUCTION

Hybrid nanoparticles[1−7] have attracted considerable attention because of their applicability in many technologically important areas such as energy conversion[8−10] and catalysis.[11−14] Au–CdS has been reported as a photocatalyst for chemical reactions,[15] most importantly for photochemical hydrogen production.[16−23] Recently, a record 100% photon-to-hydrogen production efficiency has been reported with a Pt-tipped "CdSe@CdS" rod.[24] Charge transfer from the semiconductor to the metal is very fast, less than 20 fs.[25] The possibility of changing the composition, size, shape, or other parameters of the semiconductor enables one to tailor its optical properties.[26−31] It has been shown, furthermore, that excitation of plasmons in metal nanostructures can induce the transfer of hot electrons into the semiconductors, making them interesting candidates for light harvesting materials because their absorption is tunable.[32−40] In these systems, as the metal and the semiconductor are directly in contact, the electron injection from metal to semiconductor occurs with higher efficiency. This is because the electron-transfer rate can overcome the rate of the electron–electron scattering (approximately hundreds of femtoseconds).[41] Alternatively, efficient electron transfer may occur via a plasmon-induced, metal-to-semiconductor, interfacial, charge-transfer-transition pathway as proposed by Lian and co-workers.[42] As the energy associated with the excitonic transition of CdS nanoparticles is much different from that of the surface plasmonic resonance in Au, a selective excitation of either the semiconductor or the metal domain is possible.[43]

Vela, Fang, and co-workers designed Au–CdS nanoparticles (Figure 1) and demonstrated that they were efficient photocatalysts for the conversion of amplex red to resorufin in the presence of H_2O_2.[12] Two distinct mechanisms, depending on the excitation wavelength, were identified for inducing charge separation in the nanohybrids.[12,43] Namely, either the Au or the CdS domains of the nanostructure could be selectively excited, thus changing the mechanism of resorufin production. Here, we demonstrate that there are other (simpler) means of probing this charge separation, namely, by employing ATTO dyes (for example, Figure 2), which are used extensively in single-molecule spectroscopies and super-

Received: September 28, 2016
Revised: December 13, 2016
Published: December 13, 2016

DOI: 10.1021/acs.jpcc.6b09814
J. Phys. Chem. C XXXX, XXX, XXX–XXX

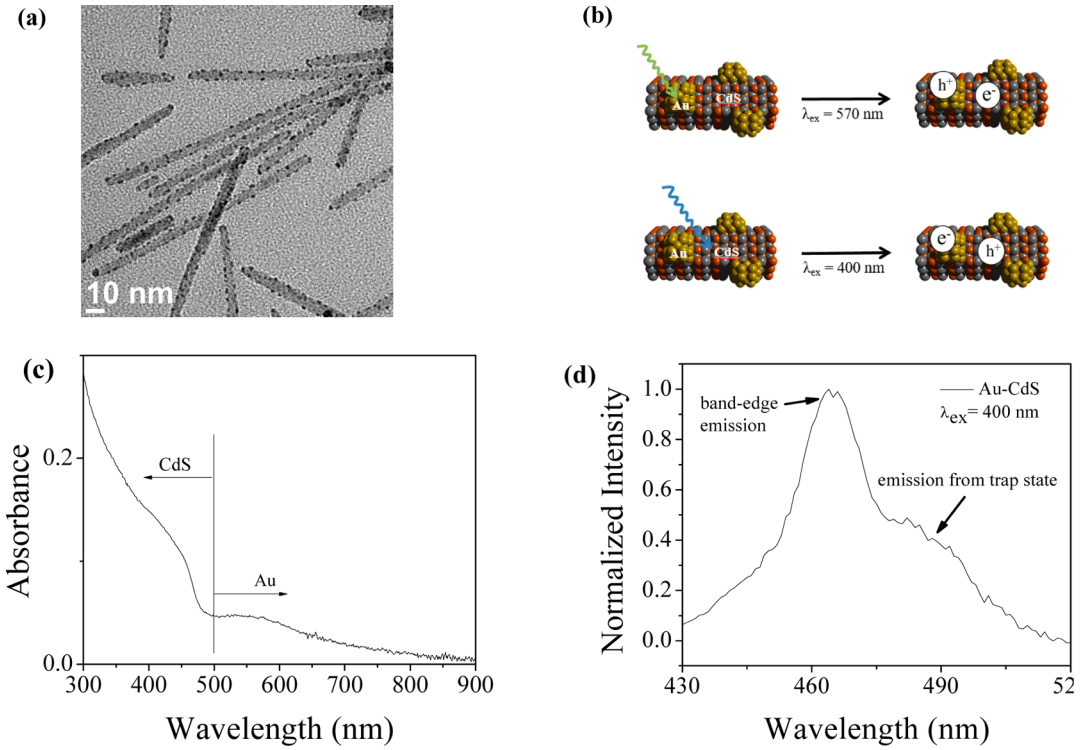

Figure 1. (a) TEM image of Au−CdS nanorods. (b) Schematic diagram of Au−CdS nanorods. With λ_{ex} = 570 nm, a charge separation takes place where the electron resides in CdS domain and the hole remains in the Au domain. When λ_{ex} = 400 nm, both the CdS and gold particles are excited. This, however, leads to charge transfer from CdS to Au. (c) Normalized absorption spectra of Au−CdS nanorods. The portion of the spectrum at wavelengths below 500 nm is mostly due to excitonic absorption of the CdS domain; that above 500 nm, from plasmonic transitions in Au domain. Thus, when λ_{ex} = 400 nm, initially the CdS domain is excited, whereas if λ_{ex} = 570 nm, the Au domain is initially excited. The extinction coefficient of the nanoparticles at 470 nm (1.3×10^6 M^{-1} cm^{-1}) has been used to measure their concentration. (d) Normalized photoluminescence spectrum of Au−CdS nanorods, λ_{ex} = 400 nm. Both the trap-state emission (a broader peak near ∼480 nm) and the narrow band-edge emission (∼465 nm) are highly quenched.

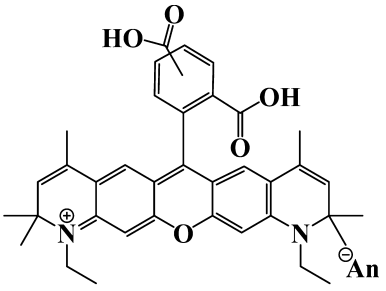

ATTO 590

Figure 2. Structure of ATTO 590. The identity of the anion, An^-, is proprietary.

resolution microscopies.[44,45] These dyes are extremely well suited as fluorescence probes for the above-mentioned techniques owing to their high fluorescence quantum yields, photostability, and large Stokes shifts. A considerable number of them covering the visible absorption and emission spectrum is commercially available. Photoinduced charge transfer is an efficient nonradiative pathway for ATTO dyes,[46] and we discuss in detail the intermolecular quenching mechanism of ATTO 590 (Figure 2a) and ATTO 655 (the structure of ATTO 655 is proprietary) with Au−CdS nanohybrids.

MATERIALS AND METHODS

Materials. ATTO 590 and ATTO 655 (free carboxy acid) were obtained from ATTO-TEC. Cadmium oxide (99.998%), sulfur (99.999%), and tetramethylammonium hydroxide pentahydrate (98%) were obtained from Alfa Aesar. Octadecylphosphonic acid (ODPA) was purchased from PCI Synthesis. Trioctylphosphine oxide (TOPO) (99%); dodecylamine (98%) and didodecyldimethylammonium bromide (98%) were purchased from Sigma-Aldrich. Trioctylphosphine (TOP) (97%) and gold(III) chloride (99%) were purchased from Strem.

Synthesis of Colloidal CdS Nanorods. We have followed the procedure described in our previous report.[47] In brief, CdO (105 mg, 0.81 mmol), TOPO (1.375 g, 3.56 mmol), and ODPA (535 mg, 0.94 mmol) were taken into a three-neck, round-bottom flask with a glass-coated stir bar. The flask, fitted with a stainless steel thermocouple, condenser, and septum was sealed and connected to a Schlenk line. The mixture was subsequently heated to 100 °C, using a heating mantle and kept under vacuum for 15 min. The apparatus was refilled with dry argon and heated to 320 °C, resulting in a colorless solution. The mixture was cooled to 120 °C, placed under vacuum for 15 min, and heated to 300 °C. TOP (1.20 mL, 2.7 mmol) was injected into the flask. The mixture was again heated to 320 °C, followed by addition of trioctylphosphine sulfide (TOPS) solution (1.00 mL, 2.2 mmol). The mixture was cooled to 315 °C for 85 min. The reaction mixture was removed from the heating mantle and cooled to room temperature. The nanorods were diluted with toluene (5 mL) and isolated by adding a 1:1 v/v 2-propanol/nonanoic acid (24 mL) mixture followed by

DOI: 10.1021/acs.jpcc.6b09814
J. Phys. Chem. C XXXX, XXX, XXX−XXX

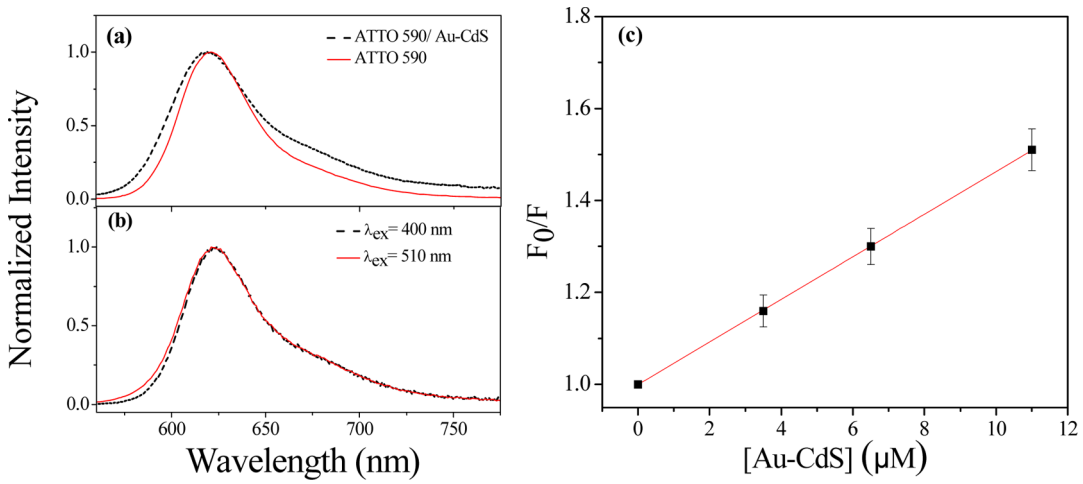

Figure 3. (a) Fluorescence spectra of ATTO 590 in the presence (black) (19 μM) and absence (red) of Au−CdS in water. This broadening was not observed with a concentration of Au−CdS below 3 μM, which can be due to detection limit of the instrument. (b) Fluorescence spectra of ATTO 590 in the presence of Au−CdS in water. λ_{ex} = 400 nm (black), λ_{ex} = 510 nm (red). (c) Stern−Volmer plot obtained from the steady-state measurement of the unquenched fluorescence intensity of ATTO 590 divided by that of the intensity of its fluorescence at a given concentration of Au−CdS, λ_{ex} = 570 nm. Stern−Volmer constant = 0.04 ± 0.01 μM^{-1}.

centrifugation (5000 rpm for 10 min). The product was redispersed in toluene.

Synthesis of Colloidal Au−CdS. The synthetic steps are briefly described below, and the detailed description can be found elsewhere.[48] The concentration of the CdS nanorod solution in toluene was estimated from its absorbance at 470 nm: $\varepsilon = 1.3 \times 10^6$ M^{-1} cm^{-1}. Fifteen milliliters of the solution was kept in a sealed three-neck, round-bottom flask, degassed, refilled with dry argon, and stored in the dark for 12 h. Gold(III) chloride ($AuCl_3$) (28 mg, 0.08 mmol), dodecylamine (117 mg, 0.63 mmol), and didodecyl dimethylammonium bromide (74 mg, 0.16 mmol) were added to 18 mL of anhydrous toluene in the dark under a dry atmosphere and sonicated for 5 min. This gold solution was injected dropwise to the CdS solution in an oil bath at 40 °C in the dark and under an argon atmosphere. Fifteen minutes after addition was complete, purification of nonvolatile products was carried out by precipitation with a 1:1 mixture of acetone and methanol (30 mL) and centrifugation (4500 rpm for 10 min). The product thus formed was redispersed in 10 mL of toluene, and 10 mL of distilled water was added. Tetramethylammonium hydroxide pentahydrate (300 mg, 1.65 mmol) and DL-mercaptosuccinic acid (50 mg, 0.33 mmol) were added, and the resulting mixture stirred overnight in the dark. The aqueous layer was separated and washed with acetone to ensure removal of excess ligands. The product was readily redispersed in water.

Electrochemical Measurements. Electrochemical measurements of the LUMO of each dye were conducted using a Pine WaveNow potentiostat with Pine screen printed electrodes (part no. RRPE1001C) composed of a 2.0 mm diameter carbon working electrode, a carbon counter electrode, and a Ag/AgCl (1 M KCl, + 0.235 V vs NHE) reference electrode. Because the Ag/AgCl reference is screen printed, it is necessary to add 1 M KCl to all solutions. Cyclic voltammetry was used to measure the LUMO of ATTO 655 (0.06 mM in aqueous 1 M KCl) by measuring five cycles each at 50 mV/s and of ATTO 590 (0.06 mM in aqueous 1 M KCl) by measuring two cycles each at 10 mV/s.

Steady-State Measurements. An Agilent 8453 UV−vis spectrometer with 1 nm resolution was used to record absorbance. Steady-state fluorescence measurements were carried out with a Spex Fluoromax-4 with a 3 or 4 nm bandpass, which was corrected for lamp spectral intensity and detector response. Concentrations were kept near 0.1 μM in all measurements to avoid reabsorption effects, reemission effects, or dye aggregation.

Lifetime Measurements. Excited-state lifetimes were determined by the time-correlated, single-photon counting (TCSPC) technique. The apparatus has been described previously.[49] The repetition rate of the fundamental (~800 nm) from a homemade, mode-locked Ti-sapphire oscillator was reduced by a Pockels cell (model 350−160, Conoptics Inc.) to 8.8 MHz. The 400 nm excitation wavelength, used for some of the experiments, was obtained from the fundamental using a U-Oplaz Technologies (Model TP-2000B) doubler/tripler. A Becker and Hickl photon counting module (model SPC-630) was used. This apparatus produces an instrument function (IRF) with a full-width at half-maximum (fwhm) of ~40−50 ps. For the experiments with λ_{ex} = 570 nm, a supercontinuum laser (Fianium Ltd.) with a 570 ± 5 nm bandpass filter was used. The repetition rate of the laser was 1 MHz; and the fwhm of the IRF, ~190 ps. A quartz cuvette of 3 mm or 1 cm path length was used. The fluorescence decays were fit to a sum of two exponentials, taking into account convolution of the IRF. Fluorescence decays were measured as a function of the concentration of Au−CdS nanoparticles, which induce a nonradiative charge-transfer process in the ATTO dye. In these experiments, similar to those in earlier work,[49] the two decays were fit globally by fixing the lifetimes and only permitting the two amplitudes to vary.

RESULTS AND DISCUSSION

Steady-State Measurements. A transmission electron-microscopy (TEM) image of CdS nanorods with deposited Au nanoparticles is given in Figure 1a. The average (±one standard deviation) length and diameter of the nanohybrids were 135 ± 10 and 6 ± 1 nm, respectively. The diameter of the gold nanoparticles was in the range 2.5−6.5 nm. A schematic diagram of the Au−CdS nanoparticles is given in Figure 1b. Their absorption spectrum is shown in Figure 1c. It is

DOI: 10.1021/acs.jpcc.6b09814
J. Phys. Chem. C XXXX, XXX, XXX−XXX

composed of the characteristic, continuous excitonic absorption from the CdS nanorods and the surface plasmon resonance band of the Au nanoparticle, thus showing that the optical properties of the original components are retained.[25,43] The retention of the CdS and Au absorption spectra permits the selective excitation of the CdS (λ_{ex} = 400 nm) or Au domains (λ_{ex} = 570 nm). Figure 1d presents the photoluminescence spectrum of the Au−CdS nanoparticles. Both the band-edge (~465 nm) and trap-state emissions (a broad emission spectrum centered around 480 nm) are highly quenched by fast (~20 fs in Au−CdS[25] and ~3.4 ps in Pt-CdS[1]) interfacial electron transfer.[1,43] The reported recombination rate is very small in Pt−CdS nano hybrids: ~1.2 ± 0.6 μs, owing to the localization of holes in CdS surface traps. Similar rates are expected for Au−CdS. Thus, during the interaction of the heterostructure with the dye, the Au−CdS particles remain essentially charge-separated. The fluorescence spectra of ATTO dyes is broadened (Figure 3a) in the presence of the Au−CdS particles, indicative of a strong electronic interaction between the two[50] or heterogeneous distribution in dielectric environment of the dye molecules when they are adsorbed transiently at the surface of the particles. Fluorescence spectra of ATTO dyes in the presence of Au−CdS do not, however, change with varying excitation wavelength (Figure 3b). The excitation spectrum of ATTO in the presence of Au−CdS agrees very well the absorption spectrum of ATTO, thus indicating the absence of ground-state aggregation (Figure S1). The decrease of fluorescence intensity with increasing Au−CdS concentration is quantified by Stern−Volmer plots with λ_{ex} = 570 (Figure 3c) or 400 nm, which yield values of 0.04 ± 0.05 and 0.15 ± 0.01 μM^{-1}, respectively.

Time-Resolved Experiments: Probing Charge Transfer from Excited-State ATTO to the Plasmonic Band of Au, λ_{ex} = 570 nm, and to the Excitonic Band of CdS, λ_{ex} = 400 nm. Time-resolved measurements provide greater insight into the charge-transfer dynamics between the ATTO dyes and the nanoparticles. Table 1 summarizes the lifetime data for ATTO dyes in the presence of Au−CdS. The fluorescence decays are well described by two decaying exponentials in which a global-fitting procedure is employed keeping the two lifetime components fixed and permitting only the amplitudes to vary.[49] In the ensuing discussion, these lifetime components are interpreted as follows. As the steady-state excitation spectra of ATTO dyes agree with the absorption spectra in the presence and absence of nanoparticles, we conclude, as mentioned above, that there is no distribution of ground-state complexes being formed and that the two lifetime components correspond to an excited-state equilibrium between two ATTO species, one of which is capable of executing excited-state charge transfer, the other which is not. (In a section of our previous paper on the quenching of ATTO 590 by tryptophan,[49] these components were erroneously and inconsistently described in terms of a ground-state equilibrium, which implies a ground-state complex, which we have demonstrated does not exist.)

Table 1. Fluorescence Quenching of ATTO Dyes by Au−CdS Nanorods

dye	λ_{ex} (nm)	τ_1 (ns)[a]	τ_2 (ns)[a]	SV constant (μM^{-1})
ATTO 590	400	3.7	0.2	0.14 ± 0.01
ATTO 590	570	3.7	0.9	0.04 ± 0.01
ATTO 655	570	1.9	1.1	0.01 ± 0.01

[a] τ_1 is the lifetime in the absence of Au−CdS; τ_2, the lifetime in its presence. Lifetime values have a ±2.5% error. The lifetime in the presence of Au−CdS does not change with the concentration of Au−CdS over the range of concentrations studied. This is similar to the quenching behavior observed with tryptophan.[49]

The dependence of the lifetime of ATTO 590 as a function of Au−CdS concentration with λ_{ex} = 570 nm is presented in Figure 4a. The shorter-lived component represents the nonradiative, charge-transfer process from ATTO 590 to the Au domain of the nanoparticle (0.93 ns); the longer-lived component, the unquenched ATTO 590 (3.7 ns) (Table SI). A Stern−Volmer plot, similar to that constructed from the steady-state data, was generated (Figure 4b), yielding a quenching constant of 0.04 ± 0.01 μM^{-1}. The absence of any ground-state complexes between Au−CdS and ATTO 590 is further confirmed by the equivalence of the Stern−Volmer plots constructed from both the time-dependent and the steady-state data.

As the extent of quenching in different ATTO dyes can change based on where they absorb, as reported by Marmé et al.,[46] and also because ATTO 655 is more frequently employed for super-resolution microscopies owing to its convenient absorption and emission properties, we carried out identical experiments on ATTO 655, which, as its name indicates, absorbs farther to the red than does ATTO 590. With λ_{ex} = 570 nm, both ATTO 655 and the Au plasmonic band are excited. We observe that, though the population of the charge-transfer species is similar to that obtained with ATTO 590 at a similar quencher concentration (Table SII), its lifetime is proportionately longer with respect to the unquenched species: 1.1 ns/1.8 ns for ATTO 655 as opposed to 0.9 ns/3.7 ns for ATTO 590, thus suggesting that there is a greater driving force for charge transfer in ATTO 590 than in ATTO 655. The Stern−Volmer plot (Figure S2) constructed with the average lifetime of ATTO 655 with varying concentration of the nanohybrid yields a Stern−Volmer constant value of 0.01 ± 0.01 μM^{-1}. Considering the relative energy of ATTO dyes (Figure 5), ATTO 590 should be quenched more, which is observed experimentally.

Similar quenching experiments were carried out with ATTO 590, λ_{ex} = 400 nm (Figure 6a). In this case, the component representing the charge transfer between ATTO 590 and Au−CdS has a lifetime of 0.2 ns (Table SIII). Hence, this observation clearly indicates that the type of charge-transfer complex formed between Au−CdS and ATTO 590 differs with the excitation wavelength: namely, 570 nm (plasmonic band of Au) and 400 nm (excitonic band in CdS). The population of the charge-separated species by excitonic excitation of CdS in Au−CdS is also much higher. The Stern−Volmer constant is about 4 times higher than that obtained when we induce excitation of the surface plasmon resonance band in the nanocomposite (Figure 6b). These observations support the observation by Lian and co-workers that photogenerated electrons and holes appear to be more active and longer-lived when generated at CdS than when generated at Au.[43] With λ_{ex} = 400 nm, the excitonic transition is excited; the nanohybrids remain charge separated with the positive charge on CdS (Figure 1b), and charge transfer to the CdS domain from the ATTO 590 is solely responsible for the quenching, which will be further discussed in the following section.

Energetics and Control Experiments. An energy-level diagram (Figure 6) was constructed from cyclic voltammetric

DOI: 10.1021/acs.jpcc.6b09814
J. Phys. Chem. C XXXX, XXX, XXX−XXX

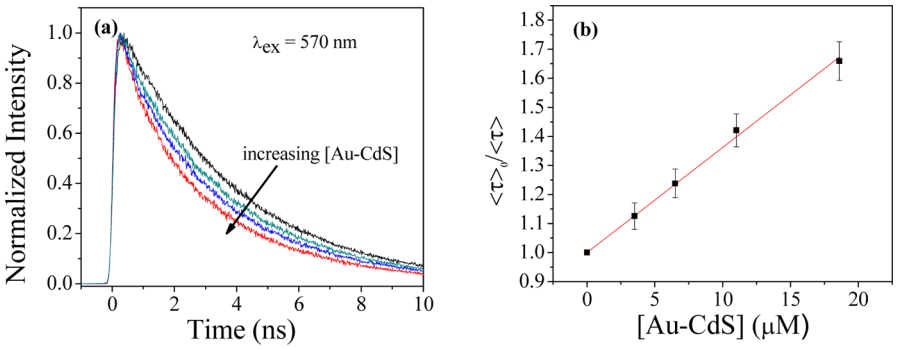

Figure 4. Stern–Volmer plot of the average lifetime of ATTO 590 as a function of [Au–CdS] (μM), λ_{ex} = 570 nm. Both the Stern–Volmer plots (based on steady-state spectra and average lifetimes) yielded the same Stern–Volmer constant of 0.04 ± 0.01 μM^{-1}.

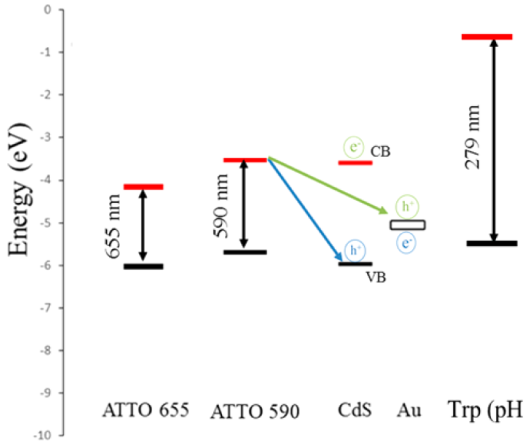

Figure 5. Energy levels of systems discussed in the text. All the energies are presented on the "absolute scale".[63] The double-headed arrows represent the maximum of absorption spectra of the dyes. CB and VB are the conduction and valence bands of CdS, respectively. The unfilled rectangle indicates ϕ, the work function of Au.[64] (The energy levels of tryptophan are included for completeness because of the similarities in quenching behavior, as discussed in the text.) The blue arrow denotes the nonradiative charge-transfer process occurring when λ_{ex} = 400 nm; the green arrow, when λ_{ex} = 570 nm. The blue and green charge pairs represent their positions in the nanoparticles with λ_{ex} = 400 nm and λ_{ex} = 570 nm, respectively.

measurements of the ATTO dyes and the reported data for CdS and Au.[43] The cathodic reduction potentials of the ATTO 590 and ATTO 655 were measured to be −3.63 and −4.15 eV vs vacuum, respectively, which correspond to the LUMO energy levels.[51−53] The HOMO energies were calculated by subtracting the excitation energies (λ_{max} of the absorption spectrum of the dyes) from the LUMO energies.[54−56] (We also attempted to obtain the molecular orbital energies of ATTO 590 via quantum chemical calculations, as briefly summarized in the Supporting Information. As, however, these calculations did not include solvent, they did not model the molecular orbital energies sufficiently accurately.) Owing to the presence of negative charge on CdS[57] with λ_{ex} = 570 nm, charge transfer from excited-state ATTO 590 to the CdS domain is unfavorable.[58] Though, on the basis of the energy level diagram, the LUMO in the ATTO dyes is very similar or lower than that of the conduction band (CB) of CdS in the nanohybrids (Figure 6), reductive charge transfer from CdS to ATTO 590 is not happening. This has been verified by a control experiment with CdS nanorods (with no gold), where the CdS is consequently uncharged. With λ_{ex} = 400 nm, we did not observe quenching with a similar concentration of CdS as that used in the experiments with the Au–CdS particles. Thus, we can conclude that in Au–CdS nanohybrids, the presence of positive charge on the CdS domain is important for efficient charge transfer from ATTO 590. The relative energy levels of the dye and of CdS valence band (because hole remains in the valence band) strongly support the assignment of charge

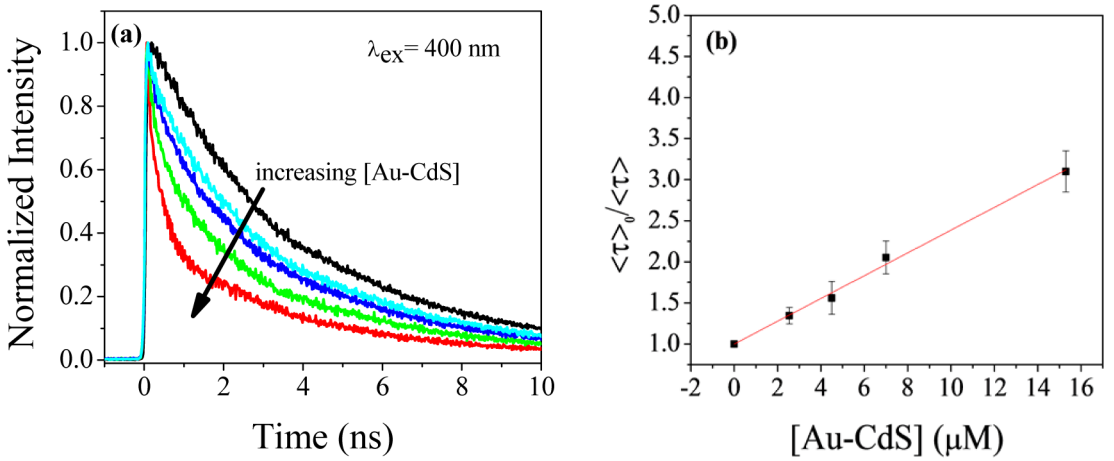

Figure 6. Stern–Volmer plot of the average lifetime of ATTO 590 as a function of [Au–CdS] (μM), λ_{ex} = 400 nm. The plot yielded a Stern–Volmer constant of 0.14 ± 0.01 μM^{-1}.

DOI: 10.1021/acs.jpcc.6b09814
J. Phys. Chem. C XXXX, XXX, XXX–XXX

transfer. As the gold domains remain negatively charged with λ_{ex} = 400 nm, as reported in the literature,[58] the charge transfer to Au becomes highly unfavorable. We estimated the free energy of charge *separation* between the Au−CdS nanoparticles and ATTO 590, with λ_{ex} = 400 nm, to be −2.39 eV compared to that with λ_{ex} = 570 nm, which we estimated to be −1.47 eV. Thus, from Marcus theory, charge separation between the Au−CdS and ATTO 590 is expected to be faster with λ_{ex} = 400 nm than that with λ_{ex} = 570 nm, though the appropriate values of the rates depend on the electronic coupling (J) between Au−CdS and the ATTO 590 and 655, which has not been reported in the literature.

Charge transfer between Au and ATTO 590 and 655 has not been documented in the literature, and there are only a few reports suggesting that charge transfer occurs from an organic dye to gold cores, and then only when short linkers (2−8 atoms) were used in polar solvents.[59,60] But owing to the presence of positive charge on the gold domains, charge transfer is favorable with λ_{ex} = 570 nm in this work.[57,58] Further, the possibility of resonance energy transfer between the dye and Au is very unlikely owing to their average separation distance[61] (∼275 Å, assuming a 20-μM concentration of the nanoparticles), as well as the poor overlap between fluorescence spectra of the dyes (mainly ATTO 655) and the plasmonic absorption. Additionally, we performed a control experiment with Au nanoparticles, which did not show quenching of fluorescence. If energy transfer were the mechanism behind the quenching with Au−CdS with λ_{ex} = 570 nm, we should have observed it in the presence of isolated Au nanoparticles. Because this was not the case, our observations are consistent with the assignment of excited-state charge transfer from ATTO 590 and 655 to the gold domain of the Au−CdS particles when λ_{ex} = 570 nm, indicating the importance of the positive charge on the Au domains for enabling facile charge transfer from the these two ATTO dyes. Additionally, based on the energy levels and the low charge-to-surface ratio in the CdS domain of the nanohybrids, there is a possibility that with λ_{ex} = 570 nm, the electron is transferring via the higher energy state of CdS and eventually going to the Au Fermi sink. Finally, we performed a control study with CdS nanorods and the two ATTO dyes with λ_{ex} = 570 nm. When λ_{ex} = 570 nm, the yield of the internal charge transfer between Au and CdS is only ∼24%.[42] Consequently, many nanohybrid moieties would be present without any charge separation in the solution when λ_{ex} = 570 nm.[12] So the quenching of ATTO 590 and 655 observed with λ_{ex} = 570 nm could be a result of charge transfer from the two ATTO dyes to the CdS domain in the particles without prior charge separation. We eliminated this possibility by performing a control experiment with λ_{ex} = 570 nm, as CdS does not absorb 570 nm. No quenching by CdS was observed, thus indicating that in the nanohybrids, quenching is not occurring owing to charge transfer between the two ATTO dyes and the CdS domain.

CONCLUSIONS

It has been shown elsewhere by using single-molecule fluorescence microscopy that the Au−CdS nanoparticles are efficient photocatalysts for the conversion of amplex red to resorufin in the presence of H_2O_2[12] and that either the Au or the CdS domains of the nanostructure could be selectively excited, thus changing the mechanism of resorufin production. Here, we demonstrate that there are other (simpler) means of probing this charge separation, namely, by employing ATTO dyes, which are used extensively in single-molecule spectroscopies and super-resolution microscopies.[44,45] These dyes are extremely well suited as fluorescence probes for the above-mentioned techniques owing to their high fluorescence quantum yields, photostability, and large Stokes shifts. A considerable number of them covering the visible absorption and emission spectrum is commercially available. Photoinduced charge transfer is an efficient nonradiative pathway for the ATTO dyes.[49,46] These properties of the ATTO dyes render them extremely promising candidates for probing such charge transfer reactions in super-resolution microscopies, such as STED, stimulated emission depletion microscopy, which we have already demonstrated in our laboratory.[44,45,62]

ASSOCIATED CONTENT

Supporting Information

The Supporting Information is available free of charge on the ACS Publications website at DOI: 10.1021/acs.jpcc.6b09814.

Excited state lifetimes, absorption and emission spectra, Stern−Volmer plot of the average lifetime vs Au−CdS concentration, CV results, optimized geometries, molecular orbitals, energy levels (PDF)

AUTHOR INFORMATION

ORCID

Javier Vela: 0000-0001-5124-6893

Jacob W. Petrich: 0000-0001-9527-6832

Present Address

[§]Department of Chemistry and Biotechnology, University of Wisconsin—River Falls, River Falls, WI, 54022, United States.

Notes

The authors declare no competing financial interest.

ACKNOWLEDGMENTS

This research is supported by the U.S. Department of Energy, Office of Basic Energy Sciences, Division of Chemical Sciences, Geosciences, and Biosciences through the Ames Laboratory. The Ames Laboratory is operated for the U.S. Department of Energy by Iowa State University under Contract No. DE-AC02-07CH11358. We thank Malinda Reichert and Pat Dilsaver for assistance with synthesis.

REFERENCES

(1) Wu, K.; Zhu, H.; Liu, Z.; Rodríguez-Córdoba, W.; Lian, T. Ultrafast Charge Separation and Long-Lived Charge Separated State in Photocatalytic CdS-Pt Nanorod Heterostructures. *J. Am. Chem. Soc.* **2012**, *134*, 10337−10340.

(2) Carbone, L.; Cozzoli, P. D. Colloidal Heterostructured Nanocrystals: Synthesis and Growth Mechanisms. *Nano Today* **2010**, *5*, 449−493.

(3) Costi, R.; Saunders, A. E.; Banin, U. Colloidal Hybrid Nanostructures: A New Type of Functional Materials. *Angew. Chem., Int. Ed.* **2010**, *49*, 4878−4879.

(4) Mokari, T.; Sztrum, C. G.; Salant, A.; Rabani, E.; Banin, U. Formation of Asymmetric One-Sided Metal-Tipped Semiconductor Nanocrystal Dots and Rods. *Nat. Mater.* **2005**, *4*, 855−863.

(5) Carbone, L.; Jakab, A.; Khalavka, Y.; Soennichsen, C. Light-Controlled One-Sided Growth of Large Plasmonic Gold Domains on Quantum Rods Observed on the Single Particle Level. *Nano Lett.* **2009**, *9*, 3710−3714.

(6) Korobchevskaya, K. G. C.; Manna, L.; Comin, A. Effect of Morphology on Ultrafast Carrier Dynamics in Asymmetric Gold−Iron

DOI: 10.1021/acs.jpcc.6b09814
J. Phys. Chem. C XXXX, XXX, XXX−XXX

Oxide Plasmonic Heterodimers. *J. Phys. Chem. C* **2012**, *116*, 26924−26928.
(7) Ruberu, T. P. A.; Nelson, N. C.; Slowing, I. I.; Vela, J. Selective Alcohol Dehydrogenation and Hydrogenolysis with Semiconductor-Metal Photocatalysts: Toward Solar-to-Chemical Energy Conversion of Biomass-Relevant Substrates. *J. Phys. Chem. Lett.* **2012**, *3*, 2798−2802.
(8) Costi, R.; Saunders, A. E.; Elmalem, E.; Salant, A.; Banin, U. Visible Light-Induced Charge Retention and Photocatalysis with Hybrid CdSe−Au Nanodumbbells. *Nano Lett.* **2008**, *8*, 637−641.
(9) Wu, K.; Lian, T. Quantum Confined Colloidal Nanorod Heterostructures for Solar-to-Fuel Conversion. *Chem. Soc. Rev.* **2016**, *45*, 3781−3810.
(10) Wu, K.; Zhu, H.; Lian, T. Ultrafast Exciton Dynamics and Light-Driven H_2 Evolution in Colloidal Semiconductor Nanorods and Pt-Tipped Nanorods. *Acc. Chem. Res.* **2015**, *48*, 851−859.
(11) Yin, H.; Wang, C.; Zhu, H.; Overbury, S. H.; Dai, S. Colloidal Deposition Synthesis of Supported Gold Nanocatalysts Based on Au−Fe_3O_4 Dumbbell Nanoparticles. *Chem. Commun.* **2008**, 4357−4359.
(12) Ha, J. W.; Ruberu, T. P. A.; Han, R.; Dong, B.; Vela, J.; Fang, N. Super-Resolution Mapping of Photogenerated Electron and Hole Separation in Single Metal−Semiconductor Nanocatalysts. *J. Am. Chem. Soc.* **2014**, *136*, 1398−1408.
(13) Alvarado, S. R.; Guo, Y.; Ruberu, T. P. A.; Tavasoli, E.; Vela, J. Inorganic Chemistry Solutions to Semiconductor Nanocrystal Problems. *Coord. Chem. Rev.* **2014**, *263*−*264*, 182−196.
(14) Alemseghed, M. G.; Ruberu, T. P. A.; Vela, J. Controlled Fabrication of Colloidal Semiconductor−Metal Hybrid Heterostructures: Site Selective Metal Photo Deposition. *Chem. Mater.* **2011**, *23*, 3571−3579.
(15) Dutta, S. K.; Mehetor, S. K.; Pradhan, N. Metal Semiconductor Heterostructures for Photocatalytic Conversion of Light Energy. *J. Phys. Chem. Lett.* **2015**, *6*, 936−944.
(16) Fujishima, A.; Honda, K. Electrochemical Photolysis of Water at a Semiconductor Electrode. *Nature* **1972**, *238*, 37−38.
(17) Gratzel, M. Photoelectrochemical Cells. *Nature* **2001**, *414*, 338.
(18) Cho, I. S.; Chen, Z.; Forman, A. J.; Kim, D. R.; Rao, P. M.; Jaramillo, T. F.; Zheng, X. Branched TiO_2 Nanorods for Photoelectrochemical Hydrogen Production. *Nano Lett.* **2011**, *11*, 4978.
(19) Shankar, K.; Basham, J. I.; Allam, N. K.; Varghese, O. K.; Mor, G. K.; Feng, X.; Paulose, M.; Seabold, J. A.; Choi, K.-S.; Grimes, C. A. Recent Advances in the Use of TiO2 Nanotube and Nanowire Arrays for Oxidative Photoelectrochemistry. *J. Phys. Chem. C* **2009**, *113*, 6327.
(20) Walter, M. G.; Warren, E. L.; McKone, J. R.; Boettcher, S. W.; Mi, Q.; Santori, E. A.; Lewis, N. S. Solar Water Splitting Cells. *Chem. Rev.* **2010**, *110*, 6446.
(21) Lewis, N. S. Toward Cost-Effective Solar Energy Use. *Science* **2007**, *315*, 798.
(22) Simon, T.; et al. Redox Shuttle Mechanism Enhances Photocatalytic H_2 Generation on Ni-Decorated CdS Nanorods. *Nat. Mater.* **2014**, *13*, 1013−1018.
(23) Wu, K. C. Z.; Lv, H.; Zhu, H.; Hill, C. L.; Lian, T. Hole Removal Rate Limits Photodriven H_2 Generation Efficiency in CdS-Pt and CdSe/CdS-Pt Semiconductor Nanorod-Metal Tip Heterostructures. *J. Am. Chem. Soc.* **2014**, *136*, 7708−7716.
(24) Kalisman, P.; Nakibli, Y.; Amirav, L. Perfect Photon-to-Hydrogen Conversion Efficiency. *Nano Lett.* **2016**, *16*, 1776−1781.
(25) Mongin, D.; Shaviv, E.; Maioli, P.; Crut, A.; U, B.; Fatti, N. D.; Vallée, F. Ultrafast Photoinduced Charge Separation in Metal-Semiconductor Nanohybrids. *ACS Nano* **2012**, *6*, 7034−7043.
(26) Saunders, A. E.; Popov, I.; Banin, U. Synthesis of Hybrid CdS−Au Colloidal Nanostructures. *J. Phys. Chem. B* **2006**, *110*, 25421−25429.
(27) Banin, U.; Ben-Shahar, Y.; Vinokurov, K. Hybrid Semiconductor−Metal Nanoparticles: From Architecture to Function. *Chem. Mater.* **2014**, *26*, 97−110.
(28) Wilker, M. B.; Schnitzenbaumer, K. J.; Dukovic, G. Recent Progress in Photocatalysis Mediated by Colloidal II-VI Nanocrystals. *Isr. J. Chem.* **2012**, *52*, 1002−1015.
(29) Vela, J. Molecular Chemistry to the Fore: New Insights into the Fascinating World of Photoactive Colloidal Semiconductor Nanocrystals. *J. Phys. Chem. Lett.* **2013**, *4*, 653−668.
(30) Wu, K.; Rodríguez-Córdoba, W.; Lian, T. Exciton Localization and Dissociation Dynamics in CdS and CdS−Pt Quantum Confined Nanorods: Effect of Nonuniform Rod Diameters. *J. Phys. Chem. B* **2014**, *118*, 14062−14069.
(31) Wu, K.; Li, Q.; Du, Y.; Chen, Z.; Lian, T. Ultrafast Exciton Quenching by Energy and Electron Transfer in Colloidal CdSe Nanosheet−Pt Heterostructures. *Chem. Sci.* **2015**, *6*, 1049−1054.
(32) Furube, A.; Du, L.; Hara, K.; Katoh, R.; Tachiya, M. Ultrafast Plasmon-Induced Electron Transfer from Gold Nanodots into TiO_2 Nanoparticles. *J. Am. Chem. Soc.* **2007**, *129*, 14852−14853.
(33) Tian, Y.; Tatsuma, T. Mechanisms and Applications of Plasmon-Induced Charge Separation at TiO_2 Films Loaded with Gold Nanoparticles. *J. Am. Chem. Soc.* **2005**, *127*, 7632−7637.
(34) Lee, J.; Mubeen, S.; Ji, X.; Stucky, G. D.; Moskovits, M. Plasmonic Photoanodes for Solar Water Splitting with Visible Light. *Nano Lett.* **2012**, *12*, 5014−5019.
(35) Chen, H. M.; et al. Plasmon Inducing Effects for Enhanced Photoelectrochemical Water Splitting: X-Ray Absorption Approach to Electronic Structures. *ACS Nano* **2012**, *6*, 7362−7372.
(36) Mubeen, S.; Hernandez-Sosa, G.; Moses, D.; Lee, J.; Moskovits, M. Plasmonic Photosensitization of a Wide Band Gap Semiconductor: Converting Plasmons to Charge Carriers. *Nano Lett.* **2011**, *11*, 5548−5552.
(37) Lee, Y. K.; Jung, C. H.; Park, J.; Seo, H.; Somorjai, G. A.; Park, J. Y. Surface Plasmon-Driven Hot Electron Flow Probed with Metal-Semiconductor Nanodiodes. *Nano Lett.* **2011**, *11*, 4251−4255.
(38) Knight, M. W.; Sobhani, H.; Nordlander, P.; Halas, N. J. Photodetection with Active Optical Antennas. *Science* **2011**, *332*, 702−704.
(39) Wu, X.; Thrall, E. S.; Liu, H.; Steigerwald, M.; Brus, L. Plasmon Induced Photovoltage and Charge Separation in Citrate-Stabilized Gold Nanoparticles. *J. Phys. Chem. C* **2010**, *114*, 12896−12899.
(40) DuChene, J. S.; Sweeny, B. C.; Johnston-Peck, A. C.; Su, D.; Stach, E. A.; Wei, W. D. Prolonged Hot Electron Dynamics in Plasmonic-Metal/Semiconductor Heterostructures with Implications for Solar Photocatalysis. *Angew. Chem., Int. Ed.* **2014**, *53*, 7887−7891.
(41) Hodak, J. H.; Martini, I.; Hartland, G. V. Spectroscopy and Dynamics of Nanometer-Sized Noble Metal Particles. *J. Phys. Chem. B* **1998**, *102*, 6958−6967.
(42) Wu, K.; Chen, J.; McBride, J. R.; Lian, T. Efficient Hot-Electron Transfer by a Plasmon-Induced Interfacial Charge-Transfer Transition. *Science* **2015**, *349*, 632−635.
(43) Wu, K.; Rodríguez-Córdoba, W. E.; Yang, Y.; Lian, T. Plasmonn-Induced Hot Electron Transfer from the Au Tip to CdS Rod in CdS-Au Nanoheterostructures. *Nano Lett.* **2013**, *13*, 5255−5263.
(44) Lesoine, M. D.; Bhattacharjee, U.; Guo, Y.; Vela, J.; Petrich, J. W.; Smith, E. A. Subdiffraction, Luminescence-Depletion Imaging of Isolated, Giant, CdSe/CdS Nanocrystal Quantum Dots. *J. Phys. Chem. C* **2013**, *117*, 3662−3667.
(45) Syed, A.; Lesoine, M. D.; Bhattacharjee, U.; Petrich, J. W.; Smith, E. A. The Number of Accumulated Photons and the Quality of Stimulated Emission Depletion Lifetime Images. *Photochem. Photobiol.* **2014**, *90*, 767−772.
(46) Marmé, N.; Knemeyer, J.-P.; Sauer, M.; Wolfrum, J. Inter- and Intramolecular Fluorescence Quenching of Organic Dyes by Tryptophan. *Bioconjugate Chem.* **2003**, *14*, 1133−1139.
(47) Reichert, M. D.; Lin, C.-C.; Vela, J. How Robust Are Semiconductor Nanorods? Investigating the Stability and Chemical Decomposition Pathways of Photoactive Nanocrystals. *Chem. Mater.* **2014**, *26*, 3900−3908.
(48) Dilsaver, P. S.; Reichert, M. D.; Hallmark, B. L.; Thompson, M. J.; Vela, J. Cu_2ZnSnS_4−Au Heterostructures: Toward Greener Chalcogenide-Based Photocatalysts. *J. Phys. Chem. C* **2014**, *118*, 21226−21234.

DOI: 10.1021/acs.jpcc.6b09814
J. Phys. Chem. C XXXX, XXX, XXX−XXX

(49) Bhattacharjee, U.; Beck, C.; Winter, A.; Wells, C.; Petrich, J. W. Tryptophan and Atto 590: Mutual Fluorescence Quenching and Exciplex Formation. *J. Phys. Chem. B* **2014**, *118*, 8471−8477.
(50) Yang, Y.; Rodríguez-Córdoba, W.; Xiang, X.; Lian, T. Strong Electronic Coupling and Ultrafast Electron Transfer between PbS Quantum Dots and TiO_2 Nanocrystalline Films. *Nano Lett.* **2012**, *12*, 303−309.
(51) Inamdar, S. N.; Ingole, P. P.; Haram, S. K. Determination of Band Structure Parameters and the Quasi-Particle Gap of CdSe Quantum Dots by Cyclic Voltammetry. *ChemPhysChem* **2008**, *9*, 2574−2579.
(52) Kucur, E.; Riegler, J.; Urban, G. A.; Nann, T. Determination of Quantum Confinement in CdSe Nanocrystals by Cyclic Voltammetry. *J. Chem. Phys.* **2003**, *119*, 2333−2337.
(53) Querner, C.; Reiss, P.; Sadki, S.; Zagorska, M.; Pron, A. Size and Ligand Effects on the Electrochemical and Spectroelectrochemical Responses of CdSe Nanocrystals. *Phys. Chem. Chem. Phys.* **2005**, *7*, 3204−3209.
(54) Bae, Y.; Myung, N.; Bard, A. J. Electrochemistry and Electrogenerated Chemiluminescence of CdTe Nanoparticles. *Nano Lett.* **2004**, *4*, 1153−1161.
(55) Amelia, M.; Lincheneau, C.; Silvi, S.; Credi, A. Electrochemical Properties of CdSe and CdTe Quantum Dots. *Chem. Soc. Rev.* **2012**, *41*, 5728−5743.
(56) Amelia, M.; Avellini, T.; Monaco, S.; Impellizzeri, S.; Yildiz, I.; Raymo, F. M.; Credi, A. Redox Properties of CdSe and CdSe−ZnS Quantum Dots in Solution. *Pure Appl. Chem.* **2010**, *83*, 1−8.
(57) Xu, W.; Jain, P. K.; Beberwyck, B. J.; Alivisatos, A. P. Probing Redox Photocatalysis of Trapped Electrons and Holes on Single Sb-Doped Titania Nanorod Surfaces. *J. Am. Chem. Soc.* **2012**, *134*, 3946.
(58) Barazzouk, S.; Kamat, P. V.; Hotchandani, S. Photoinduced Electron Transfer between Chlorophyll a and Gold Nanoparticles. *J. Phys. Chem. B* **2005**, *109*, 716.
(59) Ipe, B. I.; Thomas, K. G. Investigations on Nanoparticle−Chromophore and Interchromophore Interactions in Pyrene-Capped Gold Nanoparticles. *J. Phys. Chem. B* **2004**, *108*, 13265−13272.
(60) Ipe, B. I.; Thomas, K. G.; Barazzouk, S.; Hotchandani, S.; kamat, P. V. Photoinduced Charge Separation in a Fluorophore−Gold Nanoassembly. *J. Phys. Chem. B* **2002**, *106*, 18−21.
(61) Chandrasekhar, S. Stochastic Problems in Physics and Astronomy. *Rev. Mod. Phys.* **1943**, *15*, 1.
(62) Lesoine, M. D.; Bose, S.; Petrich, J. W.; Smith, E. A. Supercontinuum Stimulated Emission Depletion Fluorescence Lifetime Imaging. *J. Phys. Chem. B* **2012**, *116*, 7821−7826.
(63) Trasatti, S. The Absolute Electrode Potential: An Explanatory Note. *Pure Appl. Chem.* **1986**, *58*, 955−966.
(64) Mukherjee, S.; Libisch, F.; Large, N.; Neumann, O.; Brown, L. V.; Cheng, J.; Lassiter, J. B.; Carter, E. A.; Nordlander, P.; Halas, N. J. Hot Electrons Do the Impossible: Plasmon-Induced Dissociation of H_2 on Au. *Nano Lett.* **2013**, *13*, 240−247.

DOI: 10.1021/acs.jpcc.6b09814
J. Phys. Chem. C XXXX, XXX, XXX−XXX